

## STUDY OF RAMAN SCATTERING AND HALLEFFECT FOR THE $Mg_xZnO_{1-x}/n-Si$ PHOTODETECTOR

Saleem H. Trier

Department of Environment, College of Science, University of Al- Qadisiyah, Diwaniyah, Iraq

E-mail: [Salemhamza79@yahoo.com](mailto:Salemhamza79@yahoo.com)

**ABSTRACT:** In this work  $Mg_xZnO_{1-x}$  thin films have been prepared using a chemical spraying pyrolysis (CSP) technique, Mixed solutions  $Mg_xZnO_{1-x}$  have been grown at different volumetric percentages (0, 30, 50, 70, and 90)% and deposited on silicon substrates at temperatures (400, 450, and 500) °C. The crystal structure was examined by using X-ray diffraction (XRD) technique. The results showed that all the films prepared were polycrystalline, showing improvement in the crystal structure by change at temperature. Topography of the surface of the prepared films have been studied by using field emission scanning electron microscopy (FESEM), and energy dispersive X-ray spectroscopy (EDX). It showed that films contain elements (Si, N, O, Zn, and Mg) as expected. Raman scattering have been measured for  $Mg_xZnO_{1-x}/n-Si$  thin films at different Mg-content. It exhibits two intense bands at (468 and 872)  $cm^{-1}$ , corresponding to the  $E_2^{high}$  second-order Raman scattering modes, and second-order mode the  $A_1(LO)$ , is the first-order mode of ZnO. As it increases Mg-content up to (50)%, the  $A_1(LO)$  mode locate in intensity. The Hall effect have been studied, results showed measurements Hall that the pure ZnO film was negative type (n-type), while  $Mg_xZnO_{1-x}$  films were (p-type).

**KEYWORD:** Photodetector, CSP, Substrate Temperature, Raman Scattering, ZnO

### 1- THEORETICAL PART

#### 1-1 X-RAY DIFFRACTION (XRD)

X-ray diffraction peaks consist of interference construction monochrome rays reflected from any position of lattice levels at certain angles. It can calculate the distance interfaces between the levels of the diffraction angle at a certain peak by using (Bragg's law) (Kittel, C., 1976).

$$n\lambda = 2d_{hkl} \sin\theta_B \quad (1)$$

Where n integer number that represents interference degree ( $n=1, 2, 3, \dots$ ),  $\lambda$  is the wavelength of the X-ray (1.54) Å (Kittel, C. 1976),  $d_{hkl}$  is the spacing between diffracting planes and  $\theta_B$  is the Bragg's angle. Normally XRD such as:

#### 1-2 LATTICE CONSTANTS

The many crystal phases available in transparent conductive oxides (TCOs), hexagonal structure is the dominant phase in ZnO material, hexagonal phase is characterized by determining the (a and c) are lattice constants from X-ray spectrum and by using the following formula (Saremah, K., et, al, 2009), Saeed, N.M., 2011):

$$\frac{1}{d_{hkl}^2} = \frac{4}{3} \left( \frac{h^2 + hk + k^2}{a^2} \right) + \frac{1}{c^2} \quad (2)$$

Where (hkl) are Miller indices, the a-parameter is obtained from the plane (h00), while the plane (00l) is used to obtain c-parameter. In the case of cubic diamond phase such as crystallite silicon, the a-lattice constant can be obtained from (Sengupta, J., et, al, 2013):

$$\frac{1}{d_{hkl}^2} = \left( \frac{h^2 + k^2 + l^2}{a^2} \right) \quad (3)$$

#### 1-3 FULL WIDTH AT HALF MAXIMUM

The  $\beta$  of the preferred orientation (peak) could be measured, since it is equal to the width of the line profile (in radian) at the half of the maximum intensity.

#### 1-4 AVERAGE CRYSTALLITE SIZE

The single line method is one of the several line profile analysis methods based on a Voigt function to determine the size-strain parameters (microstrains and crystallite sizes). The reason behind the peak shifting was the change of stress, firstly due to the increase in temperature

additionally due to the increase in Mg- concentration. The lower boundary of the crystallite size  $D_s$  of the films was estimated using the full width at half maximum (FWHM) of (002). The average crystallite size  $D_s$ , which can be estimated using the Debye Scherer's formula (Sengupta, J., et, al, 2013).

$$D_s = \frac{k\lambda}{\beta \cos(\theta)} \quad (4)$$

Where  $k=0.94$  is the shape factor,  $\lambda$  is the wavelength of incident X-ray,  $\beta$  is the FWHM measured in radians and  $\theta$  is the Bragg's angle of diffraction peak. The FWHM of the peak corresponds to (002) plane was narrowed with increasing temperature, indicating improvement in crystallinity (Sengupta, J., et, al, 2013).

## 1-5 MICROSTRAINS

The microstrains are caused during the growth of thin films, and will be raised from stretching or compression in the lattice to make a deviation in the c-lattice constant of the hexagonal structure of the ASTM values. So the strain broadening is caused by varying displacements of the atoms with respect to their reference lattice position. This strain can be calculated from the formula (Moharram, A. H., et, al, 2014):

$$S = \frac{\beta \cos(\theta)}{4} \quad (5)$$

## 1-6 DISLOCATION DENSITY

Dislocations ( $\delta_D$ ) are an imperfection in a crystal associated with misregistry of the lattice in one part of the crystal with respect to another part. Unlike vacancies and interstitial atoms, dislocations are not equilibrium imperfections, i.e. thermodynamic considerations are insufficient to account for their existence in the observed densities. In fact, the growth mechanism involving dislocation is a matter of importance. In the present study, the dislocation density ( $\delta_D$ ) can be calculated using the following relation (Saremah, K., et, al, 2009).

$$\delta_D = \frac{1}{D_s^2} \quad (6)$$

Where  $D_s$  is the crystalline size.

## 1-7 NUMBER OF LAYERS

The number of crystalline layers ( $N_\ell$ ) which could be calculated due to the percolation theory, and it depends on

the film thickness ( $t$ ) as the relation (Ivashchenko, A. & Kerner, I. 2003):

$$N_\ell = \frac{t}{D_s} \quad (7)$$

Where  $D_s$  is a mean crystallite size or average crystallite size.

## 2- FIELD EMISSION SCANNING ELECTRON MICROSCOPY

FESEM is one of the widely instruments used in material research laboratories. Applications of FESEM include semiconductor device cross section analyses for gate widths, gate oxides, film thicknesses, construction details, small contamination feature geometry, and elemental composition measurement. Compared with convention scanning electron microscopy SEM, field emission scanning electron microscopy (FESEM) produces clearer, less electrostatically distorted images with spatial resolution down to (1.5)nm (3 to 6) times better (Allen, T., et, al, 2015).

## 3- HALL EFFECT

This phenomenon was discovered by E.T. Hall in the 1879, and known as the Hall effect Peter, (Peter, Y. Yu. & Cardona, M., 2005).

$$R_H = \frac{V_H}{I_x \cdot B_z} \quad (8)$$

$$V_H = \frac{-iB/t}{n_{eq}} \quad (9)$$

Where  $B$  is magnetic field, the Hall coefficient is defined as:

$$R_H = \frac{E_y}{j_x B} = \frac{V_H}{iB/t} = -\frac{1}{n \cdot q} \quad (10)$$

$$R_H = \frac{-n_H \mu_e^2 + p_H \mu_h^2}{q(n_H \mu_e + p_H \mu_h)} \quad (11)$$

$$R_H = \frac{1}{(p_H - n_H)q} \quad (12)$$

Hall mobility  $\mu_H$  could be calculated from the product of the conductivity  $\sigma$ , and the Hall coefficient according to the equation.

$$\mu_H = \sigma R_H \quad (13)$$

## 4- RAMAN SPECTROMETER

Raman spectrometer is a method of looking at vibration conditions in a material using monochromatic light. The activities of this technique are its ability to transmit information about the characteristic vibrations of materials, both visual and electronic.

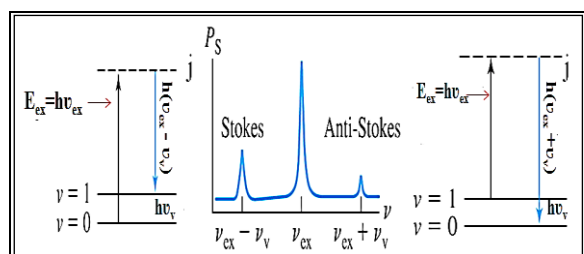


Fig. 1: The chart represents a Stokes and anti -Stokes conversion with Raman's scattering (Abdulrazzak Aldahlaki, F.H. ,2015).

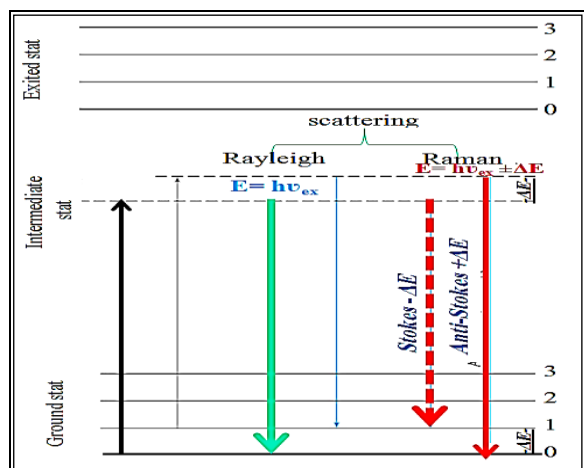


Fig. 2: A diagram showing the types of electron transport and the dispersal of Riley and Raman (Abdulrazzak Aldahlaki, F.H. ,2015).

## 2- EXPERIMENT PART

### 2-1 SILICON SUBSTRATE

Si-wafer was n-type (111) with resistivity about (1.5-5)  $\Omega$ .cm and (500  $\pm$  10)  $\mu$ m thickness. Square-shaped n-type silicon samples, each of (1.5 $\times$ 1.5)  $\text{cm}^2$  area were prepared using a steel-cut machine. Silicon wafers were washed ultrasonically in distilled water and were immersed in ethanol with a purity of (99.9)% in order to remove dirt and

oil, while native oxide layer removed by etching in dilute (2:10) HF: H<sub>2</sub>O for (3) min. the silicon wafers were cleaned in distilled water and dried in furnace at (373) K.

### 2-2 PREPARATION OF THE SPRAY SOLUTIONS

Films of Mg<sub>x</sub>ZnO<sub>1-x</sub> with different Mg-contents were deposited on a glass substrate by chemical spray pyrolysis (CSP) technique. Zinc acetate Zn(CH<sub>3</sub>COO)<sub>2</sub>.2H<sub>2</sub>O of (99.9) % purity and molecular weight equal to (219.52)g/mol and Mg acetate Mg(CH<sub>3</sub>COO)<sub>2</sub>.4H<sub>2</sub>O of (99.2) % purity and molecular weight equal to (214.46) g/mol. (x= 0,30, 50, 70, and 90)%, the deposition parameters were the same for the series of Mg<sub>x</sub>ZnO<sub>1-x</sub> thin film. The pure Zinc acetate, pure Magnesium acetate, and distilled water were mixed thoroughly to get the solution with a concentration of (0.1) M and a few drops of glacial acetic acid were then added to stabilize the solution were added to (100) mL solution to increase the solubility of the compounds. The substrate temperatures were (673,723 and 773) K during the films growth. The solution was stirred for (30)min. with a magnetic stirrer.

### 3- X-RAY DIFFRACTION (XRD)

Mg<sub>x</sub>ZnO<sub>1-x</sub> thin film such as nanocrystallite size, structure aspect layer and lattice constant have been investigated by X-ray diffraction (XRD) using Shimadzu X-ray diffractometer system (XRD-6000) which record the intensity as a function of Bragg's angle. The sample is scanned from (20-60) degree. The conditions of the system were:

- Source CuK<sub>α</sub> with radiation of wavelength  $\lambda = (1.54) \text{ \AA}$ .
- Target: Cu
- Current emission = (30) mA.
- Applied voltage = (40) KV.
- Scanning speed = (5) deg./min.

### 4 – FIELD EMISSION SCANNING ELECTRON MICROSCOPY

The morphological properties of the Mg<sub>x</sub>ZnO<sub>1-x</sub>/n-Si photodetector were investigated by (FESEM) and energy-dispersive X-ray spectroscopy (EDX). The (FESEM) is type (S-4300 of Hitachi, S-4700 FESEM) in Islamic Republic of Iran/ University of Tehran / Razi foundation. In this case, the electrons fired from the electronic gun are accelerated by an electric voltage of 15 Kv, which consists

of two magnets. There is an interaction between the atoms and electrons in the sample. This interaction causes various signals to be generated and the most commonly used signals are those from secondary back-scattered electrons. The secondary electrons are electrons of very low energy and thus, contain information of only a few angstroms deep on the surface of the layer. These electrons are then detected by a detector consisting of a scintillator-photomultiplier combination, which in turn through the system electronics drive the cathode ray tube. These images are the ones commonly used in FESEM to interpret the morphology of a sample.

## 5- HALL EFFECT MEASUREMENTS

Hall effect system (Ecola, Hall effect measurement system, HMS-3000) was used in the present study. Hall measurement is widely used in the initial characterization of semiconductor to determine the following characteristics: electrical resistivity( $\rho$ ), electrical conductivity( $\sigma$ ), carrier mobility( $\mu$ ), Hall coefficient ( $R_H$ ), carrier concentration ( $n$ ), and type carrier ( $n$  or  $p$ ).

## 6 – RAMAN SHIFT MEASUREMENTS

The Raman scattering spectroscopy (RSS) measurements for the thin film  $Mg_xZnO_{1-x}$  /n-Si photodetector were investigated by (RSS) in Islamic Republic of Iran / University of Saniti Sharif / Sharif spectroscopy laboratory. Raman spectroscopy is a spectroscopic technique based on inelastic scattering of monochromatic light, usually from a laser source. Inelastic scattering means that the frequency of photons in monochromatic light changes upon interaction with a sample. Photons of the laser light are absorbed by the sample. Frequency of the photons is shifted up or down in comparison with original monochromatic frequency, which is called the Raman effect. This shift provides information about vibrational, rotational and other low frequency transitions in

molecules. Raman spectroscopy can be used to study solid, liquid and gaseous samples.

## 3- RESULTS AND DISCUSSION

### 3- 1 (XRD) ANALYSIS OF ZnO/n-Si, AND $Mg_xZnO_{1-x}$ /n-Si THIN FILMS

Fig.1 shows the XRD spectrum of ZnO thin films grown on silicon substrate with different Mg-contents (0,30,50,70, and 90)%. At a temperature (450) °C there are three prominent diffraction peaks viz. (100), (002), and (101) which corresponding to different angle (31.65°, 34,5°, and 36.31°), respectively belong to the hexagonal wurtzite structure of ZnO has been observed see table 1. It can be concluded that the thin films deposited in these experimental conditions show strong c-axis (002) orientation growth. When mixing Mg-content ratios referred to previously, and when certain conditions arise, there are three phases, the first phase remains structure of the hexagonal wurtzite, but down the intensity of the diffraction peaks, the second phase turns into a mixture of MgO is incorporated with ZnO, the third phase turns into the cubic rock salt structure for the appearance of MgO diffraction peaks are clear. In the first case, (i.e. when the Mg-content (50)% we note the appearance of two peaks additional with directions (111),(200) corresponding to the angles of diffraction (36.87°and 42.85°), respectively. While in the third case, ( i.e. when the Mg-contents (70 and 90)% we note to increase the intensity of new peaks and the weakness of ZnO peaks and then vanish these results are consistent with research (Hullavarad, S.S. ,et , al, 2007). It remains to refer to the diffraction peaks with increase of Mg-content shifted toward larger angles. All parameters were calculated and included in the table 1. At a temperature of (450) °C we note that the peaks increasing in strength and its average crystalline size smaller. To increase content shifted toward larger angles.

Table 1: The  $G_s$ ,  $\delta_D$ ,  $S$ , and  $N_t$  of Layers data of (002),(200) Orientations for  $Mg_xZnO_{1-x}/n$ -Si at Different Mg-content, and Substrate Temperature (450) °C.

| Sample                               | Investigated line(hkl) | 2 $\theta$ (deg.) | d(nm) | FWHM ( $\beta$ ) (deg.) | Crystallite Size D(nm) | $\delta_D \times 10^{15}$ (lin m <sup>-2</sup> ) | $S \times 10^{-2}$ (lin <sup>-2</sup> m <sup>-4</sup> ) | ( $N_t$ ) |
|--------------------------------------|------------------------|-------------------|-------|-------------------------|------------------------|--|---|-----------|
| ZnO                                  | (100)                  | 31.65             | 2.823 | 0.234                   | 70.42                  | 0.2017   | 5.63  | 1.14      |
|                                      | (002)                  | 34.50             | 2.596 | 0.270                   | 61.40                  | 0.2653   | 6.47  | 1.30      |
|                                      | (101)                  | 36.31             | 2.471 | 0.200                   | 83.44                  | 0.1436   | 4.76  | 0.96      |
| Mg <sub>0.3</sub> ZnO <sub>0.7</sub> | (100)                  | 31.66             | 2.823 | 0.256                   | 62.18                  | 0.2586   | 6.38  | 1.29      |
|                                      | (002)                  | 34.65             | 2.586 | 0.307                   | 54.24                  | 0.3399   | 7.32  | 1.47      |
|                                      | (101)                  | 36.35             | 2.468 | 0.223                   | 74.70                  | 0.1792   | 5.32  | 1.07      |
| Mg <sub>0.5</sub> ZnO <sub>0.5</sub> | (100)                  | 31.75             | 2.815 | 0.246                   | 64.20                  | 0.2426   | 5.91  | 1.19      |
|                                      | (002)                  | 34.72             | 2.581 | 0.350                   | 47.56                  | 0.4421   | 8.35  | 1.68      |
|                                      | (101)                  | 36.35             | 2.468 | 0.209                   | 80.00                  | 0.1563   | 4.96  | 1.00      |
|                                      | (111)                  | 36.87             | 2.435 | 0.358                   | 46.82                  | 0.4562   | 8.48  | 1.71      |
|                                      | (200)                  | 42.85             | 2.108 | 0.387                   | 44.12                  | 0.5137   | 9.00  | 1.81      |
| Mg <sub>0.7</sub> ZnO <sub>0.3</sub> | -----                  | -----             | ----- | -----                   | -----                  | -----  | -----   | -----     |
|                                      | (002)                  | 34.75             | 2.578 | 0.325                   | 51.28                  | 0.3803   | 7.75  | 1.56      |
|                                      | (101)                  | 36.32             | 2.471 | 0.197                   | 82.76                  | 0.1460   | 4.68  | 0.99      |
|                                      | (111)                  | 36.85             | 2.436 | 0.312                   | 53.72                  | 0.3465   | 7.39  | 1.49      |
| (200)                                | 43.05                  | 2.098             | 0.357 | 47.80                   | 0.4377                 | 8.30   | 1.68  |           |
| Mg <sub>0.9</sub> ZnO <sub>0.1</sub> | -----                  | -----             | ----- | -----                   | -----                  | -----  | -----   | -----     |
|                                      | (002)                  | 34.67             | 2.584 | 0.395                   | 42.18                  | 0.5621   | 9.42  | 1.90      |
|                                      | (101)                  | 36.40             | 2.465 | 0.325                   | 51.40                  | 0.3785   | 7.72  | 1.56      |
|                                      | (111)                  | 36.87             | 2.435 | 0.442                   | 37.92                  | 0.6954   | 10.47   | 2.11      |
| (200)                                | 42.87                  | 2.107             | 0.339 | 50.36                   | 0.3943                 | 7.88   | 1.59  |           |

above represent drops of material deposited in the film, which is considered as a latent defect in the film and this seems obvious when the ratio (90)% of Mg-content.

### 3- 2 FIELD EMISSION SCANNING ELECTRON MICROSCOPY (FESEM) FOR $Mg_xZnO_{1-x}/n$ -Si FILMS

The composite  $Mg_xZnO_{1-x}/n$ -Si films were measured nanostructure in the Islamic republic of Iran/university of Tehran / Razi foundation. Surface morphologies of (FESEM) images and their corresponding (EDX) spectra at different Mg-content (0,30,50,70 and 90)%, and temperature of (450) °C are shown in the Figs.(4 A,B, C, D, and E) respectively. The morphology of the surface of pure ZnO is a nanostructure cannot determine its kind, as irregular in shape, as shown in fig.2 A. From the (FESEM) images the grain size values are found to be in the range of (30-63)nm. When add certain compensatory ratios of Mg-content into ZnO reduced surface roughness gradually as shown in figs.(4 B, C, D, and E). Decrease the grain size in the range of (26-54, 21-43, 26- 58,15-24)nm corresponding to the concentrations of Mg-contents (30,50,70, and 90)%, respectively. These values were compared with the results of XRD, as shown in table 2, these results are comparable with other results (Hullavarad, S.S. ,et , al, 2007). Grains with large sizes of (100) nm and

Table 2: Comparison between the Grain Size Calculated from (XRD) and (FESEM) Analysis for  $Mg_xZnO_{1-x}/n$ -Si Photodetector.

| Substrate Temperature(450) °C        |   |  |
|--------------------------------------|---|--|
| Contents                             | Crystallite Size Calculated from (XRD) (nm) | Grain Size Calculated from (FESEM) Images (nm) |
| ZnO (Pure)                           | 47.30                                       | 30-63  |
| Mg <sub>0.3</sub> ZnO <sub>0.7</sub> | 52.00                                       | 26-54  |
| Mg <sub>0.5</sub> ZnO <sub>0.5</sub> | 31.60                                       | 21-43  |
| Mg <sub>0.7</sub> ZnO <sub>0.3</sub> | 37.76                                       | 26-58  |
| Mg <sub>0.9</sub> ZnO <sub>0.1</sub> | 38.20                                       | 15-24  |

### 3-3 ELEMENTAL ANALYSIS FOR $Mg_xZnO_{1-x}/n$ -Si PHOTODETECTOR

The energy-dispersive X-ray analysis spectra (EDX) of the  $Mg_xZnO_{1-x}/n$ -Si photodetector deposited on silicon substrate at  $(450)^\circ\text{C}$  by (CSP) technique with different Mg-contents ( $x = 0, 30, 50, 70,$  and  $90\%$ ) are given in figs.(2 a, b, c, d and e). Among the above ratios, the ratio (30)% is the best, when measuring the concentration ratio mentioned at different temperatures was the best temperature is  $(450)^\circ\text{C}$ . Which show that all the films contain the elements (Si, N, O, Zn, and Mg) as expected, indicating formation of the  $Mg_xZnO_{1-x}/n$ -Si photodetector. Fig. 2a shows the (EDX) spectra of the (pure) ZnO film and it reveals that the compound percentage for the (Si, N, O, and Zn) are (73.16, 4.64, 12.26, and 9.94) respectively. Fig.2b depicts the (EDX) spectra of the  $Mg_{0.3}ZnO_{0.7}/n$ -Si photodetector with compound percentage for the (Si, N, O, Zn, and Mg) are (72.29, 6.82, 10.55, 6.64, and 3.70) respectively these results are similar behavior into (Shewale, P.S. & Yu, Y.S. 2016). The remaining percentages listed in table 3. The best temperature is  $(450)^\circ\text{C}$ . The (EDX) spectrum for all films are clearly observable ( $SiK\alpha$ ,  $ZnL\alpha$ ,  $MgK\alpha$ ,  $OK\alpha$  and  $NK\alpha$  lines). Lines did not show  $ZnK\alpha$ ,  $ZnK\beta$  in the (EDX) spectra. The adhesion between the  $MgZnO$  species and the Si substrate was strong, resulting in higher growth speed in the vertical direction, was the reason why the grain size of  $MgZnO$  nanoparticles was lower than those on the Si (Shewale, P.S. & Yu, Y.S. 2016). Which led to increase the intensity of spectral lines by adding Mg-content.

Table 3: Compound Percentage of the  $Mg_xZnO_{1-x}/n$ -Si Photodetector.

| MgO-<br>Contents    | Compound Percentage (%) |      |       |      |      | Total |
|---------------------|-------------------------|------|-------|------|------|-------|
|                     | Si                      | N    | O     | Zn   | Mg   |       |
| ZnO (Pure)          | 73.16                   | 4.64 | 12.26 | 9.94 | 0    | 100   |
| $Mg_{0.3}ZnO_{0.7}$ | 72.29                   | 6.82 | 10.55 | 6.64 | 3.70 | 100   |
| $Mg_{0.5}ZnO_{0.5}$ | 74.09                   | 3.92 | 11.60 | 3.55 | 6.84 | 100   |
| $Mg_{0.7}ZnO_{0.3}$ | 73.67                   | 4.57 | 11.66 | 1.40 | 8.70 | 100   |
| $Mg_{0.9}ZnO_{0.1}$ | 73.18                   | 4.69 | 12.16 | 0.52 | 9.45 | 100   |

### 3-4 HALL EFFECT MEASUREMENTS OF ZnO, AND $Mg_xZnO_{1-x}$ THIN FILMS

The resistivity of the  $Mg_xZnO_{1-x}$  thin films by (CSP) technique decreases linearly with increasing temperature indicating the semiconductor behavior. The electrical resistivity( $\rho$ ) of the  $Mg_xZnO_{1-x}$  thin films (semiconductor material), their electrical conductivity( $\sigma_{D,C}$ ), carrier

mobility( $\mu_H$ ), Hall coefficients ( $R_H$ ), carrier concentrations, and the type of the charge carrier have been calculated from Hall measurements. Hall measurements indicate that the  $Mg_xZnO_{1-x}$  thin films have two types of conductivity, pure ZnO show n-type conductivity, and the films which have contents (30,50,70, and 90)% show p-type conductivity.

Hall coefficient ( $R_H$ ) have been calculated from Hall measurements, at substrate temperature  $(400)^\circ\text{C}$ , was their value is negative for pure ZnO. ( $R_H$ ) and carrier concentration are calculated from equation(6) and the value of ( $R_H$ ) increases with the increasing of Mg-content in the films, and the values of carrier concentration decrease with the increasing of Mg-content in the films. Hall mobility is calculated from the product of the conductivity and Hall coefficient according to equation (7). It can be seen that the Hall mobility increases randomly with the increasing of Mg-content in the films at  $(400)^\circ\text{C}$ . At high temperatures  $(450,$  and  $500)^\circ\text{C}$  can observe the increases and decreases randomly in ( $n$  and  $\mu_H$ ) with Mg-content increase. The overall variation in ( $n$  and  $\mu_H$ ) can be understood in terms of the position of MgO in the ZnO lattice. The ZnO film generally grows as an n-type semiconductor, due to the presence of native defects in the form of Zinc interstitials, oxygen vacancies, or both. A decrease in ( $\mu_H$ ) at mixing concentrations may be due to the interstitial occupancy of MgO in the ZnO lattice. The presence of MgO at interstitial sites and grain boundaries in the form of oxide, besides decreasing grain size, may act as scattering centers and result in a decrease in the observed mobility at mixing concentration. Figs. (3a, b, c, and d) show the resistivity, conductivity, mobility and carrier concentration as a function of Mg-content for the  $Mg_xZnO_{1-x}$  thin films.

### 3-5 RAMAN SHIFT FOR $Mg_xZnO_{1-x}/n$ -Si AT $T_s$ (400, 450 ,and 500) $^\circ\text{C}$

Raman scatterings fig.4confirmed that synthesized  $Mg_xZnO_{1-x}/n$ -Si samples have crystalline nature with hexagonal wurtzite structure, but with obvious structural disorder induced by the preparation procedure and presence of impurities. The exact peak positions (frequency) and half-width (FWHM) of each band were determined by Raman spectrometer. To achieve the most accurate deconvolution of the obtained Raman spectra each spectrum was divided into three peaks and analyzed separately. Firstly the low-frequency region  $(468)\text{cm}^{-1}$  dominated by acoustic overtones, secondly the intermediate frequency region  $(872)\text{cm}^{-1}$  where optical and acoustic phonon combinations occur, thirdly the high-frequency region

(1306)  $\text{cm}^{-1}$  formed by optical overtones and combinations for the pure ZnO as shown in fig.4 a. The intense narrow line at (468)  $\text{cm}^{-1}$   $E_2^{\text{high}}$  second-order ZnO Raman mode-associated with the vibration of oxygen atoms, and which dominates the spectra, surely indicates that these are the scatterings from the hexagonal modification of ZnO (Ivetic, T. B., et,al,2014). Wurtzite type ZnO belongs to the space group  $C_{6v}^4$  and optical phonons belong to the following irreducible representations:  $\Gamma_{\text{opt}}=A_1+E_1+2E_2+2B_1$ . The  $A_1$  and  $E_1$  are polar modes and both Raman and infrared active,  $E_2$  are nonpolar and only Raman active, while the  $B_1$  modes are silent (Cusco, R.,et, al, 2007). Have tilted orientation the two longitudinal (LO) modes are expected to interact and create one single mode of mixed  $A_1-E_1$  symmetry known as quasi-LO mode where  $A_1-E_1$  symmetry is (872)  $\text{cm}^{-1}$ , where  $E_1(\text{LO})$  frequency is expected to show blue shift while  $A_1(\text{LO})$  is almost unaffected by Mg-mixing these results are approaching from the search results(Kilinc, N., et, al,2010). However, due to the two different crystal structures of the  $\text{Mg}_x\text{ZnO}_{1-x}/\text{n-Si}$  end members the two oxides do not show complete solid solubility, and an intermediate composition range exists in which the composite is phase separated into the wurtzite and cubic structures. For the Raman investigation of the domains with wurtzite and cubic structures, the Raman selection rules need to be considered. According to the Raman selection rules, the scattering of the LO phonon of ZnO with the wurtzite structure is allowed. In contrast, MgO with the cubic rocksalt structure has no allowed first order scattering due to the inversion symmetry of the crystal. However, defects and impurities can destroy the symmetry which in turn may result in first order Raman scattering, a phenomenon that was previously observed in MgO. As can be seen in fig.4 b, the LO mode is found to shift in frequency with Mg-content. Specifically, the LO frequency rises until (30)% Mg-content, which is attributed to the incorporation of Mg into the wurtzite structure. This is expected behavior since the LO mode of MgO is (612)  $\text{cm}^{-1}$ . Above (30)% Mg, the LO frequency is observed to saturate at (601)  $\text{cm}^{-1}$  as can be seen in fig. 4c. The saturation is attributed to the wurtzite structure becoming unable to accommodate additional Mg atoms as shown in figs.(4 d, and e). The presence of the cubic phase was confirmed previously XRD.

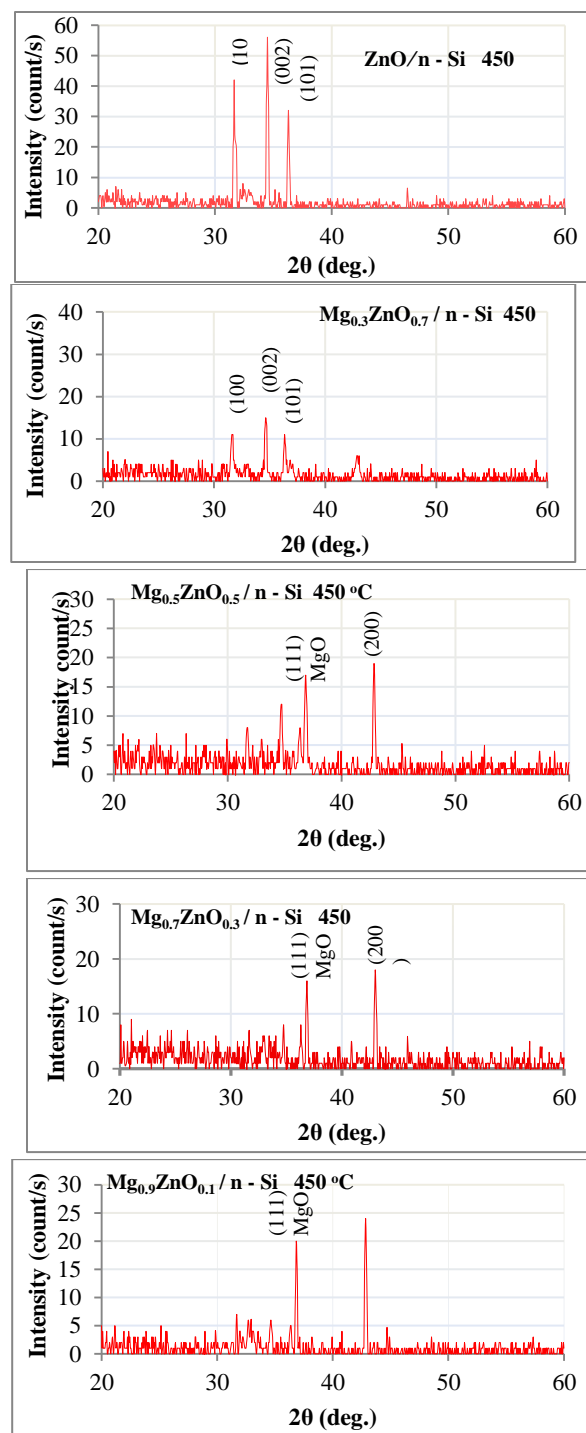


Fig.1: XRD patterns for  $\text{Mg}_x\text{ZnO}_{1-x}/\text{n-Si}$  Photodetector with Mg-contents (0,30,50,70, and 90)% and at (450) °C.

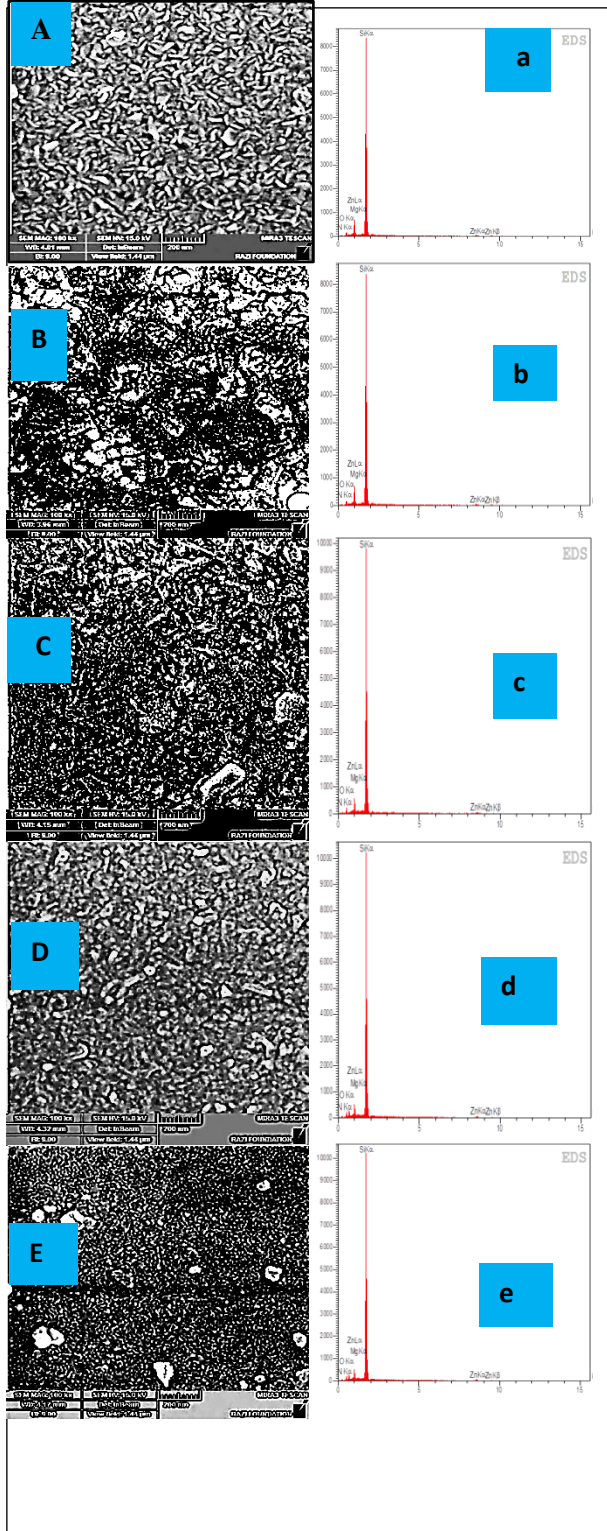


Fig.2: FESEM and EDX for  $Mg_xZnO_{1-x}/n-Si$  Photodetector for Mg-Contents (0,30,and 50,70, and 90)% Prepared, at Substrate Temperature(450) °C.

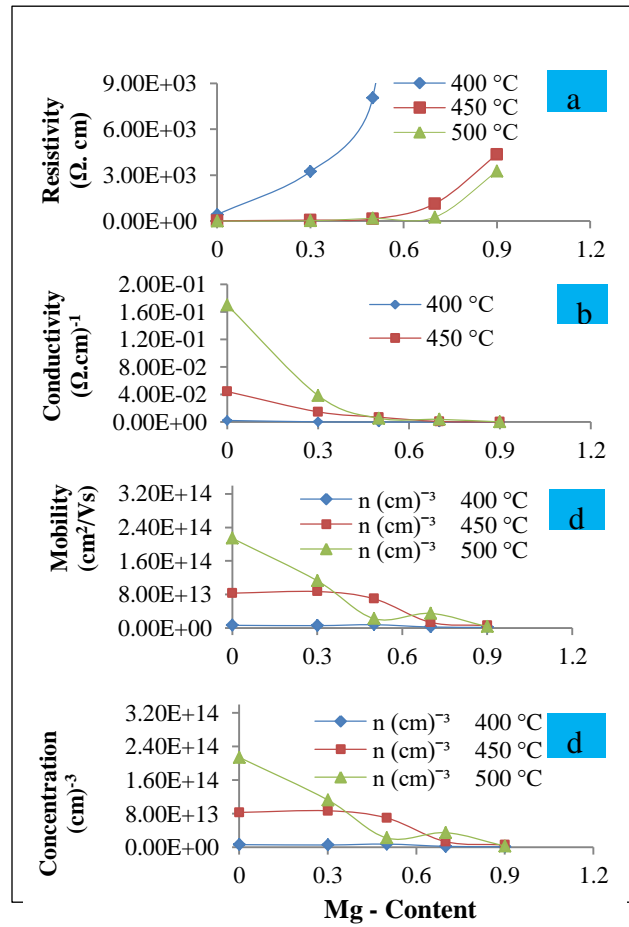


Fig.3: The  $\rho$ ,  $\sigma_{D,C}$ ,  $\mu_H$ , and  $n$  Versus Mg-Content for  $Mg_xZnO_{1-x}$  Thin Films at Different Temperatures.

### 3-5 RAMAN SHIFT FOR $Mg_xZnO_{1-x}/n-Si$ AT $T_s$ (400, 450 ,and 500) °C

Raman scatterings fig.4 confirmed that synthesized  $Mg_xZnO_{1-x}/n-Si$  samples have crystalline nature with hexagonal wurtzite structure, but with obvious structural disorder induced by the preparation procedure and presence of impurities. The exact peak positions (frequency) and half-width (FWHM) of each band were determined by Raman spectrometer. To achieve the

most accurate deconvolution of the obtained Raman spectra each spectrum was divided into three peaks and analyzed separately. Firstly the low-frequency region ( $468\text{cm}^{-1}$ ) dominated by acoustic overtones, secondly the intermediate frequency region ( $872\text{cm}^{-1}$ ) where optical and acoustic phonon combinations occur, thirdly the high-frequency region ( $1306\text{cm}^{-1}$ ) formed by optical overtones and combinations for the pure ZnO as shown in fig.4 a. The intense narrow line at ( $468\text{cm}^{-1}$ )  $E_2^{\text{high}}$  second-order ZnO Raman mode-associated with the vibration of oxygen atoms, and which dominates the spectra, surely indicates that these are the scatterings from the hexagonal modification of ZnO (Ivetic,T.B., et,al,2014). Wurtzite type ZnO belongs to the space group  $C_{6v}^4$  and optical phonons belong to the following irreducible representations:  $\Gamma_{\text{opt}}=A_1+E_1+2E_2+2B_1$ . The  $A_1$  and  $E_1$  are polar modes and both Raman and infrared active,  $E_2$  are nonpolar and only Raman active, while the  $B_1$  modes are silent (Cusco, R. ,et, al, 2007). Have tilted orientation the two longitudinal (LO) modes are expected to interact and create one single mode of mixed  $A_1-E_1$  symmetry known as quasi-LO mode where  $A_1-E_1$  symmetry is ( $872\text{cm}^{-1}$ ), where  $E_1(\text{LO})$  frequency is expected to show blue shift while  $A_1(\text{LO})$  is almost unaffected by Mg-mixing these results are approaching from the search results(Kılınç, N., et, al,2010). However, due to the two different crystal structures of the  $\text{Mg}_x\text{ZnO}_{1-x}/\text{n-Si}$  end members the two oxides do not show complete solid solubility, and an intermediate composition range exists in which the composite is phase separated into the wurtzite and cubic structures. For the Raman investigation of the domains with wurtzite and cubic structures, the Raman selection rules need to be considered. According to the Raman selection rules, the scattering of the LO phonon of ZnO with the wurtzite structure is allowed. In contrast, MgO with the cubic rocksalt structure has no allowed first order scattering due to the inversion symmetry of the crystal. However, defects and impurities can destroy the symmetry which in turn may result in first order Raman scattering, a phenomenon that was previously observed in MgO. As can be seen in fig.4 b, the LO mode is found to shift in frequency with Mg-content. Specifically, the LO frequency rises until (30)% Mg-content, which is attributed to the incorporation of Mg into the wurtzite structure. This is expected behavior since the LO mode of MgO is ( $612\text{cm}^{-1}$ ). Above (30)% Mg, the LO frequency is observed to saturate at ( $601\text{cm}^{-1}$ ) as can be seen in fig. 4c. The saturation is attributed to the wurtzite structure becoming

unable to accommodate additional Mg atoms as shown in figs.(4 d, and e). The presence of the cubic phase was confirmed previously XRD.

### 3-6 CONCLUSIONS

Through what has been discussed in the text of paper, it can be concluded the following points:

1. The addition of Mg to the films increases the her strength to withstand high temperatures and little of expansion.
2. All films have polycrystalline structure with an average crystalline size of the molecules smaller than ( $42.18\text{nm}$ ), also note the decrease in the average of crystalline size with increasing of Mg-content, this shows to the change in the structural properties of the thin films prepared.
3. Through the diagnosis of (XRD) and we found there are three phases of overlaid, the first phase remains structure of the hexagonal wurtzite, but down the intensity of the diffraction peaks, the second phase turns into a mixture of MgO is incorporated with ZnO, the third phase turns into the cubic rock salt structure and the appearance of MgO diffraction peaks are clear.
4. The structural of the ZnO films are found what dependent on the films mixed, (i.e. an increase of the mixture concentration into the film). The results of (XRD) shows that all thin films (pure and mixed) exhibit polycrystalline nature, and has the hexagonal wurtzite structure with preferential orientation in the (002) plane, when the Mg- content ratio (30)%, It turns into a cubic rock salt structure when increasing the Mg-content ratios higher than (50)% with preferential orientation in the (200).

### REFERENCES

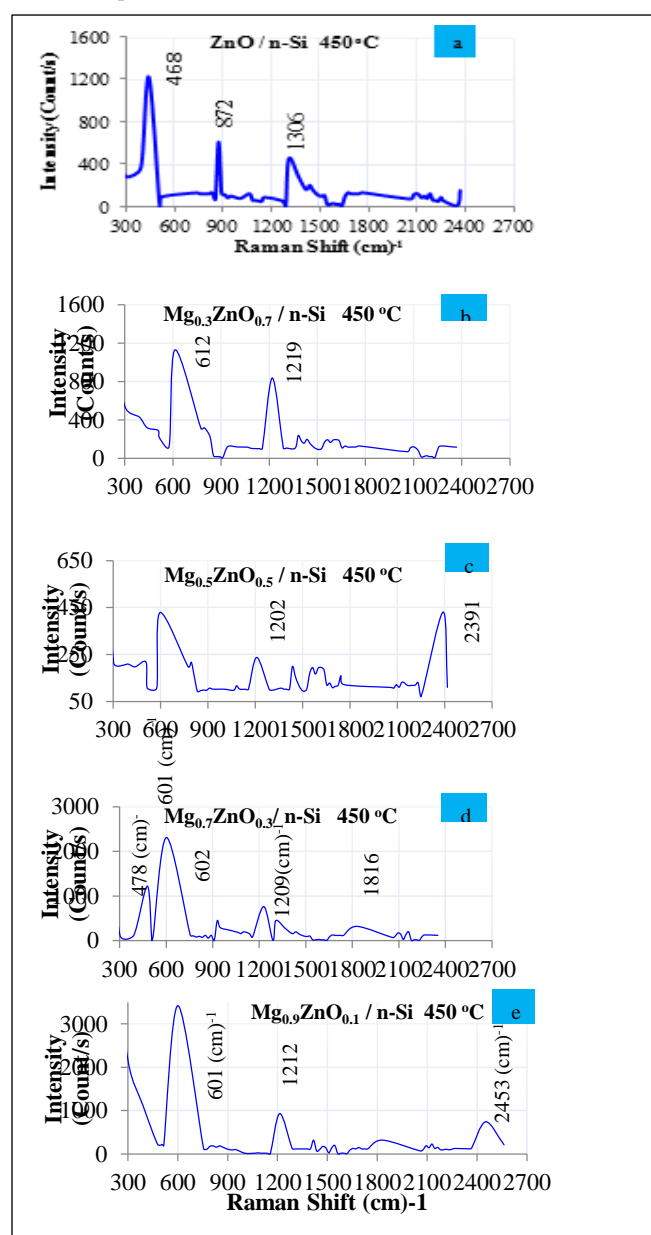
- Kittel, C. (1976). Introduction to Solid State Physics. *John. Wiley and Sons, USA*. 5<sup>th</sup> edition.
- Saremah, K., Sarma, R. & Das, H.L. (2009). Correlative assessment of structural and photoelectrical properties of thermally evaporated CdSe thin films. *Journal of Non-Oxide Glasses*, 1, 143-156.
- Saeed, N.M. (2011). Structural and optical properties of ZnS thin films prepared by spray pyrolysis technique, *Journal of Al-Nahrain University*, 14, 86-92.

Sengupta, J., Ahmed, A. & Labar, R. (2013). Structural and optical properties of post annealed Mg doped ZnO thin films deposited by the sol-gel method, *Materials Letters*, 109, 265-268.

Moharram, A. H., Mansour, S. A., Hussein, M.A. & Rashad, M. (2014). Direct precipitation and characterization of ZnO nanoparticles, *Journal of Nanomaterials*, 2014, 1-5.

Ivashchenko, A. & Kerner, I. (2003). Physical approaches to improvement of semiconductor Gas sensor based

Fig.4: Raman Shift for  $Mg_xZnO_{1-x}/n-Si$  Thin Films Prepared in Mg-contents (0,30, 50,70, and 90)%, at Substrate Temperature (450) °C.



on  $SnO_2$  thin films, *Moldavian Journal of the Physical Sciences*, 2, 95-102.

Allen, T., Rutherford, S., Murray, S., Reipert, S. & Goldberg, M. (2006). Scanning probe and scanning electron microscopy, *Elsevier Science (USA)*.

Peter, Y.Yu. & Cardona, M. (2005). Fundamentals of semiconductors, Physics and Materials Properties, *Springer*, 3<sup>rd</sup> edition, 639.

Abdulrazzak Aldahlaki, F.H., (2015). Synthesis and applications of carbon nanotubes, Ph.D. Thesis, *University of Babylon-college of science, chemistry department*.

Hullavarad, S.S., Hullavarad, N.V., Pugel, D.E., Dhar, S., Takeuchi, I. & Vispute, R. D.(2007). Homo- and hetero-epitaxial growth of hexagonal and cubic  $Mg_xZn_{1-x}O$  alloy thin films by pulsed laser deposition technique, *Journal of Physics D: Applied Physics*, 40, 4887-4895.

Shewale, P.S. & Yu, Y.S. (2016). Structural surface morphological and UV photodetection properties of pulsed laser deposited Mg-doped ZnO nanorods effect of growth time, *Journal of Alloys and Compounds*, 654, 79-86.

Ivetic, T. B., Dimitrievska, M. R., Fincur, N. L., Đacanin, L. R., Gúth, I. O., Abramovic, B.F. & Lukic-Petrovic, S. R. (2014). Effect of annealing temperature on structural and optical properties of Mg-doped ZnO nanoparticles and their photocatalytic efficiency in alprazolam degradation, *Ceramics International*, 40, 1545-1552.

Cusco, R., Lladó, E. A., Ibáñez, J. & Artús, L. (2007). Temperature dependence of Raman scattering in ZnO, *Physical Review B* 75, 1-11.

Kılinc, N., Arda, L., Öztürk, S. & Öztürk, Z.Z.(2010). Structure and electrical properties of Mg-doped ZnO nanoparticles, *Cryst. Res. Tech.*, 45, 529-53.